TISSUE ENGINEERING: Part C
Volume 21, Number 5, 2015

DOI: 10.1089/ten.tec.2014.0258

Patterning Vascular Networks *In Vivo* for Tissue Engineering Applications

Ritika R. Chaturvedi, PhD,[1] Kelly R. Stevens, PhD,[2] Ricardo D. Solorzano, BS,[1] Robert E. Schwartz, MD, PhD,[2] Jeroen Eyckmans, PhD,[3,4] Jan D. Baranski, PhD,[1] Sarah Chase Stapleton, BS,[5] Sangeeta N. Bhatia, MD, PhD,[2,6–8] and Christopher S. Chen, MD, PhD[3,4,9]

The ultimate design of functionally therapeutic engineered tissues and organs will rely on our ability to engineer vasculature that can meet tissue-specific metabolic needs. We recently introduced an approach for patterning the formation of functional spatially organized vascular architectures within engineered tissues *in vivo*. Here, we now explore the design parameters of this approach and how they impact the vascularization of an engineered tissue construct after implantation. We used micropatterning techniques to organize endothelial cells (ECs) into geometrically defined ''cords,'' which in turn acted as a template after implantation for the guided formation of patterned capillaries integrated with the host tissue. We demonstrated that the diameter of the cords before implantation impacts the location and density of the resultant capillary network. Inclusion of mural cells to the vascularization response appears primarily to impact the dynamics of vascularization. We established that clinically relevant endothelial sources such as induced pluripotent stem cell-derived ECs and human microvascular endothelial cells can drive vascularization within this system. Finally, we demonstrated the ability to control the juxtaposition of parenchyma with perfused vasculature by implanting cords containing a mixture of both a parenchymal cell type (hepatocytes) and ECs. These findings define important characteristics that will ultimately impact the design of vasculature structures that meet tissue-specific needs.

Introduction

Tissue engineering has yielded significant advancements in the treatment of a variety of diseases caused by tissue damage or dysfunction.[1] While highly promising, a critical limitation in the field is the successful vascularization of large tissue constructs.[2] *In vivo*, it is estimated that a cell must be located within 150–200 μm of the nearest capillary to survive and function optimally.[3] Due to this constraint, current efforts to implant large engineered tissue structures are hindered by significant cell death in areas that exceed this diffusion limit due to insufficient delivery of oxygen and nutrients and waste removal.[1,2] The future utility of engineered tissues depends on the successful development of vascular architectures within the constructs that mimic the complexity of native tissues and lead to easy integration with host circulation.

In vivo, native tissue comprised specialized cells and vasculature embedded within a tissue-specific extracellular matrix in a highly organized manner. The liver, in particular, has a precisely defined microarchitecture involving a complex interplay between hepatocyte cords and microvessel networks that is thought to impact metabolic mass transport and tissue function.[4] Indeed, it is the loss of this architecture due to replacement by fibrotic tissue and regenerative nodules that defines chronic cirrhosis.[5] Successful therapeutic tissue engineering will rely on our ability to recapitulate such macrostructural organization by integrating architecturally defined vascular networks with tissue-specific cellular structures.

We have recently established a novel approach for creating functional spatially organized vascular architectures within engineered tissues *in vivo*.[6] Our approach uses micropatterning techniques to organize endothelial cells (ECs)

[1]Department of Bioengineering, School of Engineering and Applied Science, University of Pennsylvania, Philadelphia, Pennsylvania.
[2]Harvard-MIT Health Sciences and Technology, Institute for Medical Engineering and Science, Massachusetts Institute of Technology, Cambridge, Massachusetts.
[3]Department of Biomedical Engineering, Boston University, Boston, Massachusetts.
[4]Wyss Institute for Biologically Inspired Engineering, Harvard University, Boston, Massachusetts.
[5]Department of Chemical and Biological Engineering, School of Engineering and Applied Science, University of Pennsylvania, Philadelphia, Pennsylvania.
[6]Howard Hughes Medical Institute, Cambridge, Massachusetts.
[7]Department of Electrical Engineering and Computer Science, Massachusetts Institute of Technology, Cambridge, Massachusetts.
[8]David H. Koch Institute for Integrative Cancer Research, Massachusetts Institute of Technology, Cambridge, Massachusetts.
[9]Department of Medicine, Brigham and Women's Hospital, Harvard Medical School, Boston, Massachusetts.

into geometrically defined ''cords,'' which in turn act as a template after implantation for the guided formation of patterned capillaries that integrate with the host tissue. In this study, we provide an important insight into the utility of this method for robustly vascularizing tissue engineering constructs by exploring which design parameters influence the ultimate vascularization of the construct. Specifically, we characterize the effect of cord geometry, mural cell composition, and EC source on the vascularization response after implantation. Finally, we demonstrate the ability to control the geometry of engineered tissue by implanting cords containing both a parenchymal cell type (hepatocytes) and ECs, leading to tight juxtaposition of parenchyma with perfused vasculature following implantation.

Materials and Methods

Fabrication of PDMS templates and preparation of engineered implants

Endothelial cell cords were micropatterned as previously described.[6,7] Cells (ECs and 10T1/2s at a 50:1 ratio unless otherwise stated) were suspended in 2.5 mg/mL liquid rat tail collagen type I (BD Biosciences) and centrifuged into poly(dimethylsiloxane) (PDMS) channels (150 μm channels unless otherwise stated) pretreated with 0.01% Pluronic F127 (Fig. 1). Excess unpolymerized collagen and cells were removed by dewetting the surface of the substrate. The collagen was polymerized, a growth medium was added, and constructs were incubated at 37°C for 4–6 h to enable cord formation. Cords were then removed from the PDMS substrates by inverting onto a drop of unpolymerized 10 mg/mL bovine fibrin (Sigma-Aldrich). After the fibrin was polymerized, the PDMS was removed and a second layer of unpolymerized fibrin added and polymerized to fully encase the cords. The embedded cords were cut with a 6-mm biopsy punch before implantation. To include hepatocytes, primary human hepatocytes, J2-3T3 fibroblasts, and endothelial cells were mixed in a 1:1:1 ratio before centrifugation.

In vivo *implantation of constructs*

All surgical procedures were conducted according to protocols approved by the University of Pennsylvania or Massachusetts Institute of Technology Institutional Animal Care and Use Committee. Eight-week-old female Nu/nu nude mice (Charles River) or NCr nude mice (Taconic) were anesthetized using isoflurane and the constructs were sutured to the mesenteric parametrial fat pad. The incisions were closed aseptically, and animals were administered 0.1 mg/mL buprenorphine every 12 h for 3 days following surgery.

Statistical analysis and quantification of vascularization parameters

Quantification was performed manually on imaged hematoxylin and eosin (H&E) sections using FIJI Open Source Software. Blood area was quantified by measuring the total area tissue containing blood within a cord. Measurements were normalized to average cord area to compensate for oblique cutting angles. The vessel number was quantified by counting individual vessels within a cord and then normalized to the average cord area. The vessel diameter was quantified by measuring the diameter of individual vessels within a cord. Sections for quantification were chosen from the center of the constructs, and a minimum of three sections at least 150 μm apart were quantified per cord. All data are expressed as the mean ± standard error. Statistical significance was determined using a one-way analysis of variance (ANOVA) followed by Tukey's *post hoc* test for group comparisons.

For more detailed methods, please see Supplementary Data (Supplementary Data are available online at www.liebertpub.com/tec).

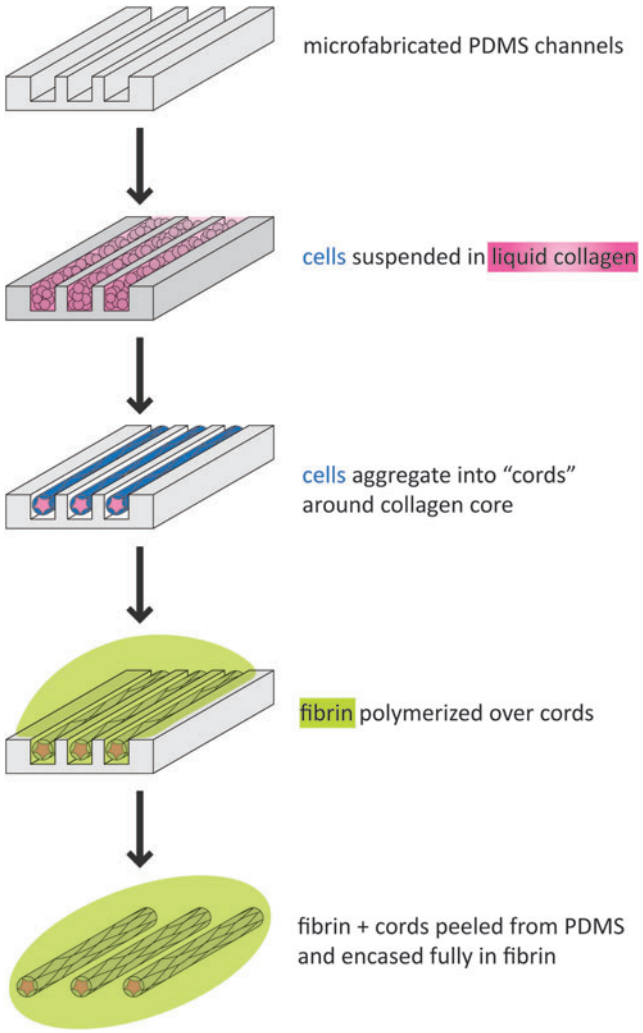

FIG. 1. Microfabrication of cords. Schematic representation of the processes used to generate cords. Collagen, *pink*; cells, *blue*; fibrin, *green*. PDMS, poly(dimethylsiloxane). Color images available online at www.liebertpub.com/tec

Results

Endothelial cord diameters can be tailored to manipulate capillary density and location within engineered tissue

The ability to tailor vascular location and density within engineered tissue is essential to meet the varying metabolic burdens of diverse parenchymal cell types. We have previously described that preformed cords within a construct

induced rapid vascularization upon implantation.[6] In this study, we explored whether modulating the initial diameter of the cords impacts the geometry of the resultant vasculature formed *in vivo*. We implanted tissue constructs containing cords formed from 50, 150, and 500 μm PDMS channels. Upon formation, the cords contracted to roughly 50% of PDMS channel width in average diameters of 25, 75, and 250 μm (Fig. 2A). All samples were punched with a 6-mm biopsy punch before implantation to preserve uniformity in length. In all conditions, H&E staining of samples resected 7 days postimplantation (PI) confirmed the presence of red blood cells (RBCs) present around the perimeter of the cords within capillary-like cellular structures (Fig. 2B). Sirius red/Fast green staining demonstrated persistence of a collagen core within the cords for all conditions (Fig. 2C). The diameter of this collagen core was proportional to the initial cord diameter for different cord sizes.

To better assess the vascularization response, we quantified the surface area of blood, the total number of vessels, and the diameter of vessels in H&E-stained sections (Fig. 2D). This quantification suggested that the average vessel diameter remained relatively constant across all constructs, with the 500 μm cord condition exhibiting slightly larger vessels. All vessels in all conditions were small-diameter vessels that remained within the defined ''capillary''[8] range and appeared to track along the surface perimeter around the cords. The surface area of blood within a cord remained similar throughout the conditions with roughly 20–25% of the cord surface containing blood. This finding indicates that there is more blood, overall, in samples containing larger cords and less blood in samples containing smaller cords. The number of capillaries per cord increased with an increasing cord diameter, although this number decreased per cross-sectional area of cord since the larger collagen core remained unvascularized. Therefore, the resultant blood vessels and, hence, blood are more dense and localized in implants containing small cords and more dispersed in implants containing larger cords. Overall, our data indicate that the diameter of the cords does not substantially affect the diameter of the resultant vessels, but strongly determines the location and density of the resultant vessels and the overall amount of blood present within an engineered tissue. Therefore, the cord diameter could be used to tailor the localization and density of capillaries to meet specific needs for various parenchymal tissues.

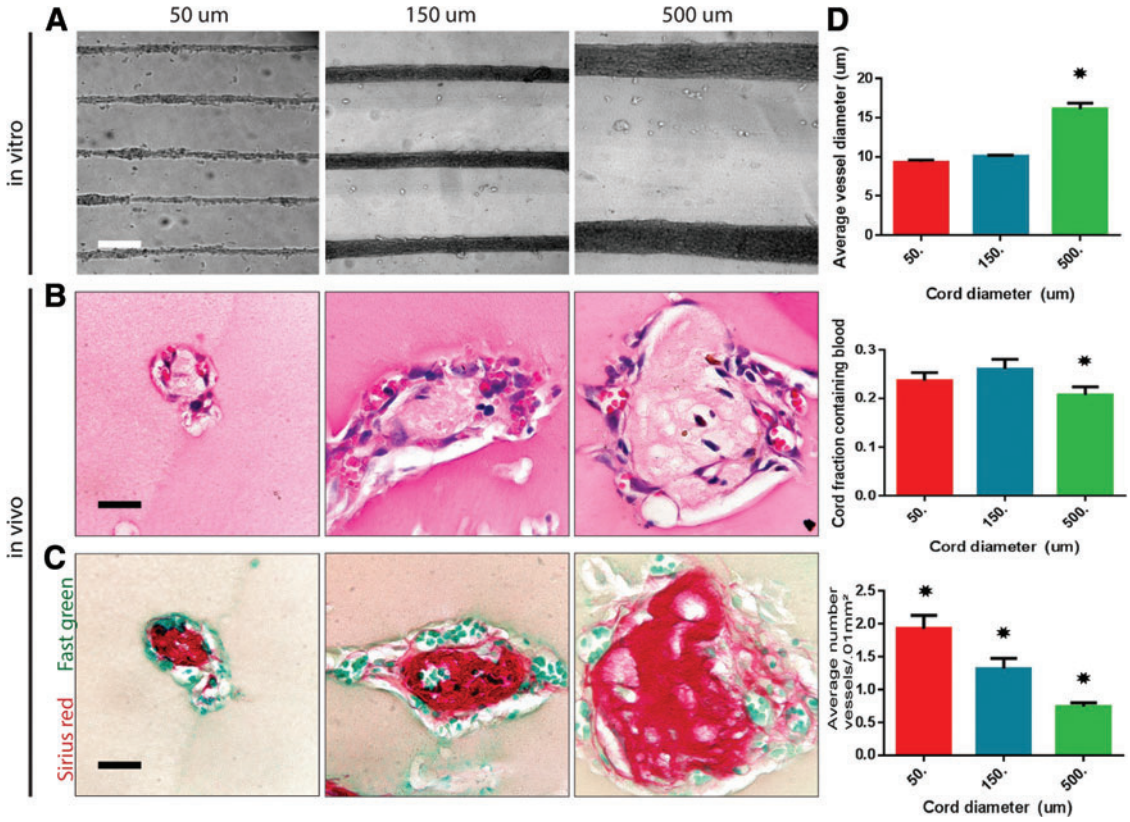

FIG. 2. Cord diameters can be tailored to manipulate capillary density and location within engineered tissue. **(A)** Phase images of endothelial cell (EC) cord constructs made from varying PDMS channels (50, 150, and 500 μm) and after removal from PDMS substrate and embedded within fibrin gel (scale bar, 250 μm). **(B)** Hematoxylin and eosin (H&E) staining of implanted tissue containing cords of varying diameters (50, 150, and 500 μm) resected after 7 days *in vivo* suggests the presence of blood in small vessels along the perimeter of the cords (scale bar, 50 μm). **(C)** Sirius red/Fast green staining of collagen within the cords after harvest (scale bar, 50 μm). **(D)** Quantification of blood area, vessel diameter, and vessel numbers for varying cord diameters. $*p < 0.05$ for comparison. Error bars: SEM, $n \geq 20$, one-way ANOVA followed by Tukey's *post hoc* test. ANOVA, analysis of variance; SEM, standard of the mean. Color images available online at www.liebertpub.com/tec

Endothelial cells are necessary to drive the vascularization response in vivo

Many groups have demonstrated that a mixture of mural and endothelial cells is required for robust vascularization and viability of randomly cocultured cells within engineered vascular implants.[9–14] It has been hypothesized that the presence of mural cells increases networking and tubulogenesis of endothelial cells, which in turn aids in anastomosis to the host upon implantation.[10–14] However, because geometrically patterning endothelial cells into cords results in very rapid networking *in vitro* and robust vascularization upon implantation, the mural cell requirements within the system may be different. To determine the contribution of mural cells (10T1/2s) to capillary formation after implantation, cords composed of EC:10T1/2 ratios of 0:1, 1:2, 5:1, 50:1, and 1:0 (holding total cell number constant) were implanted and resected 7 days PI. The vascularization response appears to require endothelial cells, as H&E staining of implanted cords of 10T1/2s alone showed no evidence of blood 7 days PI (Fig. 3A). Likewise, H&E staining of

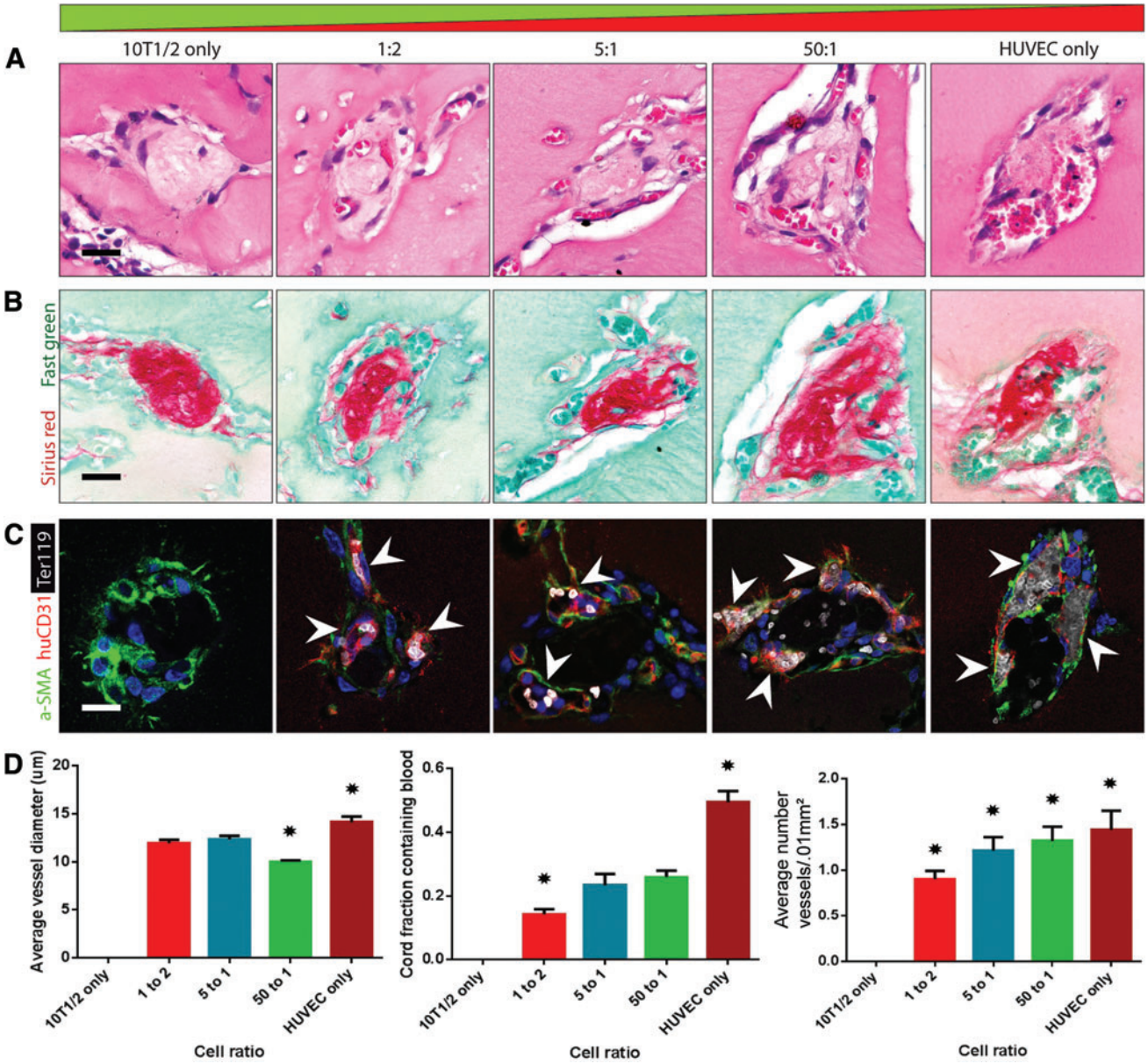

FIG. 3. Endothelial cells in cords are necessary to drive engraftment and integration to host. **(A)** H&E staining of cords consisting of various EC:10T1/2 ratios (10T1/2 only, 1:2, 5:1, 50:1, HUVEC only) resected after 7 days *in vivo* suggests the presence of blood in small vessels along the perimeter of all cord conditions containing endothelial cells (scale bar, 50 μm). **(B)** Sirius red/Fast green staining of collagen within the cords after harvest (scale bar, 50 μm). **(C)** Ter-119 (erythrocytes, *white*), human-specific CD31 (HUVECs, *red*), and alpha-smooth muscle actin (α-SMA; pericytes, *green*) staining positively identify red blood cells (RBCs) and ECs (*arrowheads*: individual vessels) and suggest that vessels consist of implanted human endothelium with perivascular colocalization (scale bar, 50 μm). **(D)** Quantification of blood area, vessel diameter, and vessel numbers for varying cell ratios. *A p-value of <0.05 for comparison. Error bars SEM, $n \geq 20$, one-way ANOVA followed by Tukey's *post hoc* test. HUVEC, human umbilical endothelial cells. Color images available online at www.liebertpub.com/tec

implanted cords of another commonly used mural source, primary human mesenchymal stem cells, resected at 7 days PI did not demonstrate any evidence of blood (Supplementary Fig. S1). In all other conditions containing endothelial cells (including those without mural cells), RBCs were present around the perimeter of the cords within capillary-like cellular structures (Fig. 3A). Sirius red/Fast green staining confirmed the presence of collagen within the cords for all conditions (Fig. 3B).

To confirm the presence of RBCs and human ECs, tissue sections were immunohistochemically stained for Ter-119, an erythroid cell marker and human-specific CD31 (Fig. 3C, arrowheads). Ter-119 staining demonstrated the presence of RBCs in all conditions containing endothelial cells in localized patterns matching those previously observed with H&E staining. Human ECs circumscribed the RBCs and were found in all conditions containing implanted endothelial cells, suggesting the formation of blood vessels containing implanted human ECs. Staining for alpha-smooth muscle actin (α-SMA) revealed the presence of α-SMA-positive cells in tight association with ECs in all cord conditions, suggesting a pericyte phenotype. Interestingly, implanted cords containing human umbilical endothelial cells (HUVECs) only (without 10T1/2s) also stained positive to the same extent for α-SMA at 7 days PI, suggesting host invasion of pericyte-like cells upon engraftment.

Quantification (Fig. 3D) demonstrated that the average vessel diameter remained relatively constant across all cell ratios with the 100% EC condition exhibiting slightly larger vessels. The surface area of blood within a cord increased slightly with the increasing EC ratio, with a significant rise in the 100% EC condition (from 25% to 50% of total cord area). The number of capillaries per cord also increased with the increasing EC ratio. To examine whether the slight differences in vascularization response were due to variability in contractility among different cell compositions, we assessed the cord contractility *in vitro* for ECs and EC:10T1/2 at a 1:1 ratio (Supplementary Fig. S2). Our study suggests that by 4–6 h (time of embedding and implantation), no differences are detectable that would explain the *in vivo* response. Together, these results suggest that ECs are necessary for the vascularization response and the increasing number of ECs within an implant appears to enhance the number of vessels and blood within the construct. However, although the number of ECs has a positive influence on vascularization, the effect is relatively small as the vascularization response in samples containing 33–98% ECs is largely comparable. Thus, in a tissue engineering context, the approach may provide some flexibility to introduce other cell types while still having sufficient ECs to induce vascularization, although further functional experiments would be necessary to validate this.

Cords composed of clinically relevant endothelial cells support the vascularization response

The ultimate goal of tissue engineering is to create clinically viable engineered tissues that can be used therapeutically in human patients. While useful in demonstrating proof of principal in vascular engineering strategies, HUVECs are not widely considered a compatible source of ECs for clinical translation.[15] Therefore, the use of clinically relevant ECs such as human microvascular endothelial cells (HMVECs) that are easily obtained through patient skin biopsies or induced pluripotent stem cell-derived ECs (iPS ECs), which can be isolated and created from patient-specific cell sources is an important consideration in determining the translational viability of this approach. To determine whether more clinically relevant ECs induce a similar vascularization response as HUVECs, we implanted HMVECs and iPS ECs and resected 7 and 14 days PI. Before implantation, iPS ECs were generated based on previously described protocols[16,17] and verified to express endothelial markers and respond to endothelial-specific stimuli (Supplementary Fig. S3). The iPS ECs responded to the proangiogenic gradient by invading the surrounding matrix as multicellular lumen-containing sprouts (Supplementary Fig. S3A), as previously demonstrated by human umbilical vein endothelial cells.[18] The iPS EC angiogenic sprouts exhibit classic EC expression of the cell junctional protein and platelet endothelial cell adhesion molecule (CD31) and confirmed correct apical–basal polarization, as indicated by the CD34 apical marker podocalyxin immunofluorescence (Supplementary Fig. S3B).

H&E staining of resected tissues containing HUVEC-only cords, HMVEC-only cords, and iPS EC cords suggested the presence of RBCs around the perimeter of the cords at 7 days PI. Large areas of blood were present at 7 days PI and were surrounded by a fragmented layer of cells, reminiscent of the pattern observed in leaky vasculature (Fig. 4A). Loose cellular structures were replaced over time by smaller, more definitive vessel-like cellular lining stereotypical of mature microvessels by 14 days PI in all conditions (Fig. 4D). Sirius red/Fast green staining demonstrated the presence of collagen within the cords for all conditions and time points (Fig. 4B, E). Ter-119 staining confirmed the presence of RBCs in all conditions and time points in localized patterns matching those previously observed with H&E staining (Fig. 4C, F, arrowheads). Human ECs circumscribed the RBCs and were found in all conditions and time points, suggesting the formation of blood vessels containing implanted ECs. HuCD31 staining also demonstrated the presence of larger vessels in all cell conditions at 7 days and smaller more capillary-like vessels at 14 days. The huCD31 staining was slightly less robust at 14 days in HMVEC and iPS EC conditions, although this did not affect the overall vascularization response. Interestingly, although the implanted cords did not contain an initial population of mural cells, α-SMA-positive cells were found in tight association with ECs in all conditions and time points. Furthermore, α-SMA-positive staining appeared to be located on the apical side of the vessels at 7 days (Fig. 4C, arrowheads) and on the basal side at 14 days (Fig. 4F, box), possibly suggesting an intravascular host origin of pericyte-like cells upon engraftment and perfusion. We have previously shown that the vessels induced by EC:10T1/2 cords are extensively perfused.[6] To confirm that this also occurs in the EC-only cords, we performed systemic injections of human-specific lectin (*Ulex europaeus* agglutinin 1 [UEA-1]—TRITC) through the tail vein at 2 weeks following implantation of HUVEC-only cords. Visualization of cryosections demonstrated that 8 out of 10 explants contained perfused vessels with human-specific endothelial cells, similar to the percentage of samples that contain erythrocytes by histological assessment of

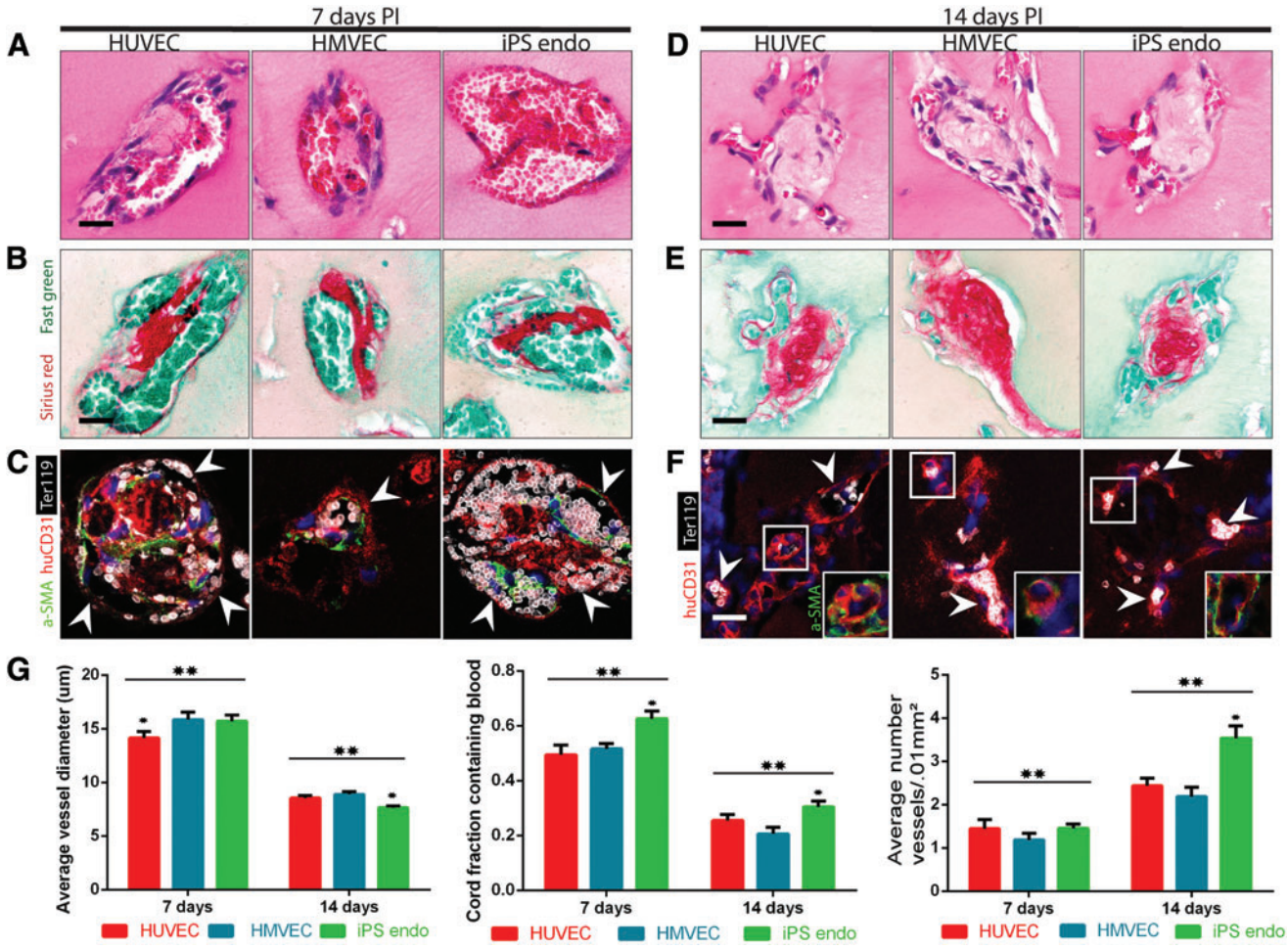

FIG. 4. Translational cell types. **(A)** H&E staining of cords composed of HUVECs, human microvascular endothelial cells (HMVECs), and induced pluripotent stem cell-derived ECs (iPS ECs) resected after 7 days and **(D)** 14 days *in vivo* suggests the presence of blood in large vessels at 7 days that organize into small capillaries by 14 days (scale bar, 50 μm). **(B)** Sirius red/Fast green staining of collagen within the cords resected after 7 days and **(E)** 14 days *in vivo*. **(C)** Ter-119 (erythrocytes, *white*), human-specific CD31 (human ECs, *red*), and α-SMA (pericytes, *green*) staining positively identify RBCs and ECs and suggest that vessels consist of implanted human endothelium with perivascular colocalization at 7 days (*arrowheads*: individual vessels) and **(F)** 14 days postimplantation (PI) [*arrowheads*: individual capillaries, *box*: α-SMA (pericytes, *green*); scale bar, 50 μm]. **(G)** Quantification of blood area, vessel diameter, and vessel numbers for translational cell types at different time points. *A p-value of <0.05 for comparison. Error bars SEM, $n \geq 20$, one-way ANOVA followed by Tukey's *post hoc* test. **A p-value of <0.05 for comparison of each group between time points. Error bars SEM, $n \geq 20$, t-test. Color images available online at www.liebertpub.com/tec

human CD31 vessels containing Ter199$^+$ blood at this time point (76%).

Quantification (Fig. 4G) suggests that the vascularization response is similar among the different cell types and that without mural cells, maturation of vessels occurs within the cords between 7 and 14 days PI, during which the area of blood within cords decreases, the number of capillaries per cord increases, and the average vessel diameter decreases. Together, these results suggest that engineered cords composed of different sources of potentially patient-specific endothelial cells can induce host vascularization and perfusion, which occur through the initial formation of large nascent vessels that later lumenize and reorganize into smaller, more numerous, and mature capillaries that are organized around and alongside the collagen core of the cords.

Hybrid cords of ECs and hepatocytes induce the formation of patterned engineered tissue integrated with host vasculature

Because cord formation is driven by contractility,[6] and fewer than 50% of the cord may be composed of ECs, we hypothesized that virtually any cell type could be added to the EC suspension to create hybrid EC/parenchymal cell cords. Therefore, we next sought to determine whether engineered tissue containing hepatocytes cocultured with ECs within the cords themselves would become vascularized. We hypothesized that delivery of hepatocytes in cords may result in better recapitulation of native tissue architecture, in which hepatocytes are organized along hepatic sinusoids in cord-like structures.[4] To assess whether endothelial cords would support primary human hepatocytes after implantation, tissue

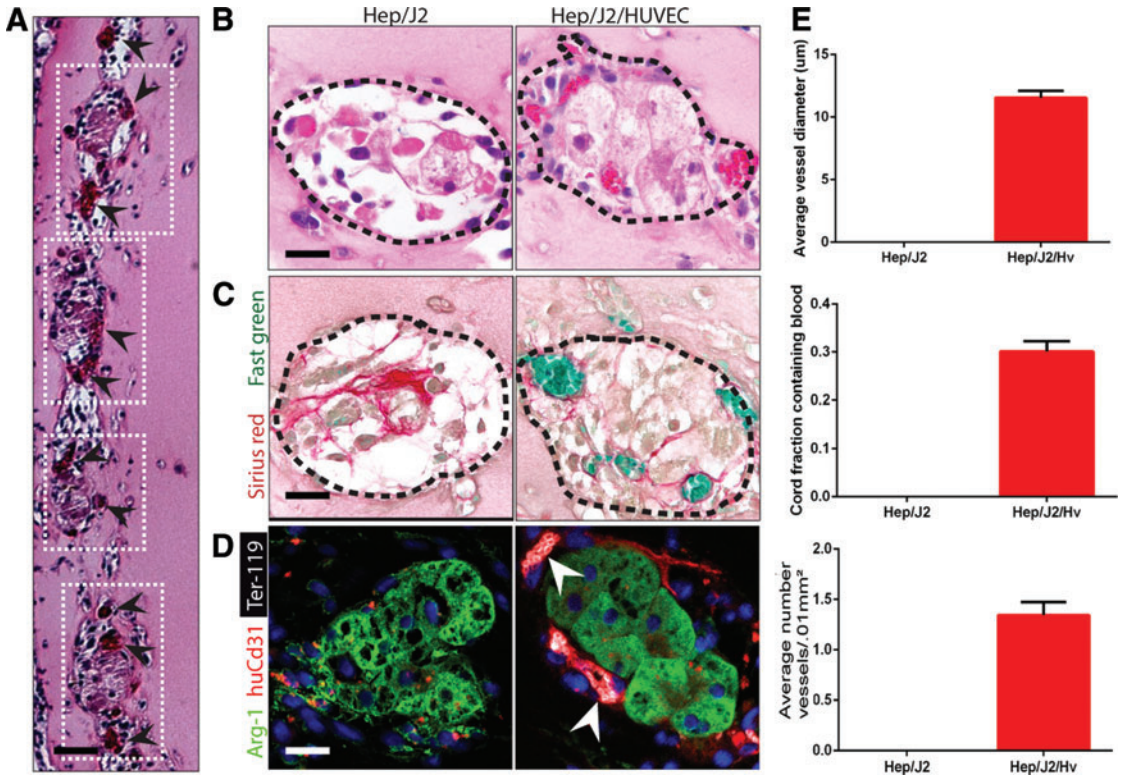

FIG. 5. Hybrid cords. **(A)** H&E staining of cord-containing tissue constructs resected after 7 days *in vivo* (*boxes*: location of individual cords, *arrowheads*: individual capillaries around periphery of cord). **(B)** H&E staining of cords made of hepatocytes only and hybrid Hep/EC cords resected after 7 days *in vivo* suggests the presence of blood in small vessels along the perimeter (*dotted line*) of the hybrid cords. **(C)** Sirius red/Fast green staining of collagen within cords suggests that the hepatocytes largely degrade the collagen core. **(D)** Ter-119 (erythrocytes, *white*), human-specific CD31 (HUVECS, *red*), and arginase 1 (Arg-1; hepatocytes, *green*) confirm the presence of blood encased in capillaries lined with human endothelium directly adjacent to viable hepatocytes in the hybrid cord condition (*arrowheads*: individual capillaries; scale bar, 50 μm). **(E)** Quantification of blood area, vessel diameter, and vessel numbers for hybrid cords. Error bars SEM, $n \geq 20$. Color images available online at www.liebertpub.com/tec

constructs containing human hepatocytes cocultured 1:1 with HUVECs during cord formation, or hybrid cords were sutured to the parametrial fat pad in athymic mice and were compared with control constructs containing cords made of hepatocytes alone. Histological assessment of tissues explanted at 7 days PI revealed the presence of localized cell laden structures within the fibrin implant that were organized spatially into patterns mimicking the original position of the implanted cords (Fig. 5A). Higher magnification elucidated the presence of RBCs around the perimeter of the cord-like structures in the hybrid EC/Hep cords, while showing that the Hep-only cords were devoid of RBCs (Fig. 5B). The peripheral localization of host vasculature suggested that ECs and Heps self-sorted within the cord structure, with the ECs migrating to the perimeter of the cords, and encasing a hepatocyte core. Sirius red/Fast green staining confirmed that the presence of hepatocytes leads to degradation of the collagen cores of the cords, particularly in the coculture case, in which no remnants of the collagen core were evident upon resection (Fig. 5C). Immunofluorescent staining for RBCs, human ECs, and viable hepatocytes (Ter-119, huCD31, and arginase 1 [Arg-1], respectively) demonstrated the presence of perfused neovessels directly adjacent to hepatocytes in the hybrid cord condition (Fig. 5D, arrowheads). Furthermore, hepatocytes were located no farther than 150 μm from the nearest capillary.

Quantification (Fig. 5E) demonstrated the complete lack of blood and vessels in implanted cords containing hepatocytes only. In the hybrid cord condition, on average, 30% of the cord cross-sectional surface area contained blood. Together, the data suggest that hybrid cords lead to a very intimate association of neovessels with hepatic tissue within cords, with no collagen cores.

Discussion

Patterning vascular and parenchymal architectures within an engineered tissue is currently a critical limitation to our ability to create complex metabolically active tissues such as the kidney and liver.[19] We recently described a novel method of patterning endothelial cells into cords that act as a template for guided vascularization upon implantation *in vivo*.[6] In this study, we explore the design parameters that will be important for the future utility of this method for the vascularization of clinically relevant parenchymal tissues. First, we demonstrate that a varying cord diameter does not lead to changes in the caliber of host vessels that form. This finding is consistent with developmental vasculogenesis, during which large vessels generally grow in size over a period of time and do not form spontaneously.[20] Instead, we find that the cord diameter can tailor the location and density

of capillaries formed in the construct and could therefore be used to impact engineered tissue vascularization. It is remarkable that the formation of these vessels occurs in the absence of any parenchymal demand. Given the endogenous feedback control systems for regulating capillary density, we therefore might anticipate that these supraphysiologic vessels may ultimately destabilize and involute unless a parenchymal cell were in place to support capillary demand. Conversely, if a highly metabolic implant ultimately requires a much higher capillary density than can be induced by our approach, it is possible that the initial gains due to cords may still leave a tissue undervascularized. Thus, tissue-specific long-term studies will need to be undertaken to better understand the downstream effects of this approach.

Many different cell types have been used historically in vascular tissue engineering strategies.[9–14,21–23] Initially, HUVECs alone were implanted, followed by the discovery that coimplanting HUVECs with a supporting mural cell led to a more stable vasculature *in vivo*.[11] Others discovered that preculturing HUVECs and fibroblasts *in vitro* for a number of days before implantation led to increased networking and more robust vascularization *in vivo*.[10,12,13] Additionally, C3H10T1/2s have been previously shown to increase networking behavior and vascularization due to differentiating into smooth muscle alpha-actin expressing pericytes.[24] Collectively, these studies suggest that supporting mural cells are essential for proper EC networking within randomly seeded implants *in vivo*. Based on this literature, our previous studies used a 1:50 ratio of 10T1/2s and HUVECs. With this ratio, we found that large leaky vessels formed within the cords by 3 days PI and later reorganized into smaller, more numerous capillaries around the periphery of the cords. Our quantification data suggested that this switch occurred sometime between 5 and 7 days PI.[6] In our studies here, we varied the percentage of 10T1/2s to elucidate the exact contribution of mural cells within our system. We found that increasing the percentage of 10T1/2s within the cords from 2% to 66% decreased the total blood within the cord slightly. Eliminating 10T1/2s altogether led to the formation of fewer large vessels at 7 days PI. However, by 15 days PI, these larger vessels again remodeled into smaller, more numerous capillaries. Surprisingly, even without the initial inclusion of 10T1/2 cells, the vessels within the implant stained positive for α-SMA, suggesting that pericyte-like cells are recruited to the implant from host circulation upon anastomosis and establishment of blood flow. This finding is consistent with previous studies, which illustrate that circulating perivascular progenitor cells contribute to tumor angiogenesis.[25] Together, these results imply that the presence of 10T1/2s does not impact the overall vascularization effect in our system, but rather the timeline of maturation from large vessels to smaller stable capillaries.

Previous studies indicate that ECs of different origins exhibit different vascularization responses *in vivo*.[15] In this study, we demonstrated that clinically relevant cell types such as HMVECs and iPS ECs induced a similar vascularization response to HUVECs upon implantation *in vivo*. Again, without a supporting mural cell, implanted cords containing HMVECs and iPS ECs formed a few large vessels at 7 days which later reorganized into smaller, more numerous capillaries by 14 days. It was also apparent that iPS ECs had a slight advantage over other cell types in the total volume of blood. Because the vascularization effect is similar among these different EC types, our system can be customized by using patient-specific (syngeneic) endothelial cells. Taken together, our findings that cords can support vascularization with a range of endothelial cell sources and stoichiometries also might provide sufficient flexibility to allow for the customization of engineered tissue with tissue-specific endothelial cells, or sourcing focused on more accessible tissues (e.g., skin), as well as variation in the ratios of parenchymal cells, supporting cells, and endothelial cells depending on the context. Whether cords composed of tissue-specific ECs could provide better support for specific parenchyma in this approach remains to be seen.

We also demonstrate our ability to pattern parenchymal cells within the cords themselves. In our previous studies, hepatocytes were seeded into a fibrin matrix either without exogenous ECs or in the bulk of the matrix surrounding cords, leaving a large fraction of parenchymal cells outside the predicted perfusion zone of the cords.[6] In this study, hepatocytes and ECs contracted together to form cords, keeping the parenchymal cells in close proximity to the host vascularization response. Furthermore, coculturing ECs and hepatocytes within cords led to sorting of the cell types within the cords with ECs forming a sheath around a hepatocyte core. These studies are in their infancy, and future studies to elucidate the effects of scaling the size of implants, as well as the paracrine and juxtacrine signaling effects of the two cell types within these conformations and their effects on functional outputs such as albumin and urea will be necessary for clinical applications. The patterning approach offered here will add to others[26] to allow the study and optimization of such effects using multiple cell and tissue types *in vitro* to inform future *in vivo* studies. Ultimately, the ability to control vascular architecture using methods demonstrated here will enable studies of the effects of vascular features such as vessel density, alignment, and branching on tissue oxygenation and function and will inform the next generation of custom tissue-specific vascular architectures.

Acknowledgments

Research reported in this publication was supported by the National Institute of Biomedical Imaging and Bioengineering of the National Institutes of Health under Award Number EB000262 and EB08396. The content is solely the responsibility of the authors and does not necessarily represent the official views of the National Institutes of Health. S. Bhatia is a Howard Hughes Investigator. Individual fellowship support was provided by a NIH NRSA (K.R.S., 1F32DK091007; R.R.C., 5T32AR007132-35).

Disclosure Statement

No competing financial interests exist for all authors.

References

1. Vacanti, J.P., and Langer, R. Tissue engineering: the design and fabrication of living replacement devices for surgical reconstruction and transplantation. Lancet **354,** S32, 1999.
2. Lovett, M., Lee, K., Edwards, A., and Kaplan, D.L. Vascularization strategies for tissue engineering. Tissue Eng Part B Rev **15,** 353, 2009.

3. Jain, R.K. Transport of molecules, particles, and cells in solid tumors. Annu Rev Biomed Eng **1,** 241, 1999.
4. Reid, L.M., Fiorino, A.S., Sigal, S.H., Brill, S., and Holst, P.A. Extracellular matrix gradients in the space of Disse: relevance to liver biology. Hepatology **15,** 1198, 1992.
5. Ishibashi, H., Nakamura, M., Komori, A., Migita, K., and Shimoda, S. Liver architecture, cell function, and disease. Semin Immunopathol **31,** 399, 2009.
6. Baranski, J.D., Chaturvedi, R.R., Stevens, K.R., Eyckmans, J., Carvalho, B., Solorzano, R.D., Yang, M.T., Miller, J.S., Bhatia, S.N., and Chen, C.S. Geometric control of vascular networks to enhance engineered tissue integration and function. Proc Natl Acad Sci U S A **110,** 7586, 2013.
7. Raghavan, S., Nelson, C.M., Baranski, J.D., Lim, E., and Chen, C.S. Geometrically controlled endothelial tubulogenesis in micropatterned gels. Tissue Eng Part A **16,** 2255, 2010.
8. Dragneva, G., Korpisalo, P., and Ylä-Herttuala, S. Promoting blood vessel growth in ischemic diseases: challenges in translating preclinical potential into clinical success. Dis Models Mech **6,** 312, 2013.
9. Koike, N., Fukumura, D., Gralla, O., Au, P., Schechner, J.S., and Jain, R.K. Tissue engineering: creation of long-lasting blood vessels. Nature **428,** 138, 2004.
10. Levenberg, S., Rouwkema, J., Macdonald, M., Garfein, E.S., Kohane, D.S., Darland, D.C., Marini, R., van Blitterswijk, C.A., Mulligan, R.C., D'Amore, P.A., and Langer, R. Engineering vascularized skeletal muscle tissue. Nat Biotechnol **23,** 879, 2005.
11. Au, P., Tam, J., Fukumura, D., and Jain, R.K. Bone marrow-derived mesenchymal stem cells facilitate engineering of long-lasting functional vasculature. Blood **111,** 4551, 2008.
12. Stevens, K.R., Kreutziger, K.L., Dupras, S.K., Korte, F.S., Regnier, M., Muskheli, V., Nourse, M.B., Bendixen, K., Reinecke, H., and Murry, C.E. Physiological function and transplantation of scaffold-free and vascularized human cardiac muscle tissue. Proc Natl Acad Sci U S A **106,** 16568, 2009.
13. Chen, X., Aledia, A.S., Ghajar, C.M., Griffith, C.K., Putnam, A.J., Hughes, C.C., and George, S.C. Prevascularization of a fibrin-based tissue construct accelerates the formation of functional anastomosis with host vasculature. Tissue Eng Part A **15,** 1363, 2008.
14. Chen, X., Aledia, A.S., Popson, S.A., Him, L., Hughes, C.C., and George, S.C. Rapid anastomosis of endothelial progenitor cell-derived vessels with host vasculature is promoted by a high density of cotransplanted fibroblasts. Tissue Eng Part A **16,** 585, 2009.
15. Barclay, G.R., Tura, O., Samuel, K., Hadoke, P.W., Mills, N.L., Newby, D.E., and Turner, M.L. Systematic assessment in an animal model of the angiogenic potential of different human cell sources for therapeutic revascularization. Stem Cell Res Ther **3,** 1, 2012.
16. Si-Tayeb, K., Noto, F.K., Nagaoka, M., Li, J., Battle, M.A., Duris, C., North, P.E., Dalton, S., and Duncan, S.A. Highly efficient generation of human hepatocyte-like cells from induced pluripotent stem cells. Hepatology **51,** 297, 2010.
17. James, D., Nam, H.S., Seandel, M., Nolan, D., Janovitz, T., Tomishima, M., Studer, L., Lee, G., Lyden, D., Benezra, R., Zaninovic, N., Rosenwaks, Z., Rabbany, S.Y., and Rafii, S. Expansion and maintenance of human embryonic stem cell-derived endothelial cells by TGF [beta] inhibition is Id1 dependent. Nat Biotechnol **28,** 161, 2010.
18. Nguyen, D.H.T., Stapleton, S.C., Yang, M.T., Cha, S.S., Choi, C.K., Galie, P.A., and Chen, C.S. Biomimetic model to reconstitute angiogenic sprouting morphogenesis *in vitro*. Proc Natl Acad Sci U S A **110,** 6712, 2013.
19. Vacanti, J.P. Tissue engineering and the road to whole organs. Br J Surg **99,** 451, 2012.
20. Adams, R.H., and Alitalo, K. Molecular regulation of angiogenesis and lymphangiogenesis. Nat Rev Mol Cell Biol **8,** 464, 2007.
21. Au, P., Daheron, L.M., Duda, D.G., Cohen, K.S., Tyrrell, J.A., Lanning, R.M., Fukumura, D., Scadden, D.T., and Jain, R.K. Differential *in vivo* potential of endothelial progenitor cells from human umbilical cord blood and adult peripheral blood to form functional long-lasting vessels. Blood **111,** 1302, 2008.
22. Ghajar, C.M., George, S.C., and Putnam, A.J. Matrix metalloproteinase control of capillary morphogenesis. Crit Rev Eukaryot Gene Expr **18,** 251, 2008.
23. Melero-Martin, J.M. *et al.* Engineering robust and functional vascular networks *in vivo* with human adult and cord blood-derived progenitor cells. Circ Res **103,** 194, 2008.
24. Hirschi, K., Rohovsky, S., and D'Amore, P. PDGF, TGF-beta, and heterotypic cell cell interactions mediate endothelial cell-induced recruitment of 10T1/2 cells and their differentiation to a smooth muscle fate. J Cell Biol **141,** 805, 1998.
25. Mancuso, P., Martin-Padura, I., Calleri, A., Marighetti, P., Quarna, J., Rabascio, C., Braidotti, P., and Bertolini, F. Circulating perivascular progenitors: a target of PDGFR inhibition. Int J Cancer **129,** 1344, 2011.
26. Stevens, K.R., Ungrin, M.D., Schwartz, R.E., Ng, S., Carvalho, B., Christine, K.S., Chaturvedi, R.R., Li, C.Y., Zandstra, P.W., Chen, C.S., and Bhatia, S.N. InVERT molding for scalable control of tissue microarchitecture. Nat Commun **4,** 1847, 2013.

Address correspondence to:
Christopher S. Chen, MD, PhD
Department of Biomedical Engineering
Boston University
36 Cummington Mall
Boston, MA 02215

E-mail: chencs@bu.edu

Received: May 6, 2014
Accepted: October 14, 2014
Online Publication Date: February 12, 2015

Supplementary Data

Supplementary Materials and Methods

Cell culture

Primary human umbilical endothelial cells (HUVECs, Lonza) were maintained on 0.1% gelatin-coated dishes in EGM-2 (Lonza). C3H10T1/2 cells [American Type Culture Collection (ATCC)] were maintained in low-glucose Dulbecco's modified Eagle's medium (DMEM) containing 10% fetal bovine serum (FBS; Atlanta Biologicals), 100 units/mL penicillin, and 100 mg/mL streptomycin (Invitrogen). Primary dermal human microvascular endothelial cells (HMVEC-ds; Lonza) were maintained on 0.1% gelatin-coated dishes in EGM-2 MV (Lonza). Primary human hepatocytes from a 1-year-old female Caucasian donor (Lot Hu8085; CellzDirect) were maintained in high-glucose DMEM (Cellgro) containing 10% FBS (Gibco), 1% (vol/vol) ITS supplement (BD Biosciences), 0.49 pg/mL glucagon, 0.08 ng/mL dexamethasone, 0.018 M HEPES, and 1% (vol/vol) penicillin–streptomycin (pen–strep; Invitrogen). J2-3T3 fibroblasts (gift of Dr. Howard Green; Harvard Medical School) were maintained in high-glucose DMEM containing 10% bovine serum, 100 units/mL penicillin, and 100 mg/mL streptomycin.

iPSC culture and endothelial-like cell differentiation

Undifferentiated induced pluripotent stem cells (iPSCs) were maintained as described.[1] In brief, iPSCs were cultured in monolayer on Matrigel (Becton Dickinson) in the human embryonic stem cell (ESC) medium conditioned by mouse embryonic fibroblasts (Global Stem). The human ESC culture medium consisted of Advanced DMEM/F12 (Gibco) supplemented with 20% knockout serum replacement (Invitrogen), 1 × nonessential amino acids (Gibco), 1 × L-glutamine (Invitrogen), 1 × penicillin/streptomycin (Invitrogen), 1 × β-mercaptoethanol (Gibco), and 4 ng/mL FGF-2 (Invitrogen). Human pluripotent stem cells were then grown to confluency on Matrigel (BD Biosciences) and then incubated in 5 units/mL dispase (Gibco) until colonies were completely detached from the substrate. These colonies were washed and cultured in the hESC medium on ultralow attachment plates (Corning) for 24 h. Embryoid bodies were then cultured as described[2] in the hESC base medium without FGF-2. The medium was supplemented with 20 ng/mL BMP4 (R&D Systems) (removed at day 7); on day 1, the medium was supplemented with 10 ng/mL ActivinA (R&D Systems) (removed at day 4); on day 2, the medium was supplemented with 8 ng/mL FGF-2 (Invitrogen) (remained for the duration of culture); on day 4, embryoid bodies were transferred to adherent conditions on Matrigel-coated plates and the medium was supplemented with 25 ng/mL VEGF-A (Invitrogen) (which remained for the duration of culture); on day 7, SB431542 (Tocris) was added at 10 μM concentration and remained for indicated duration. Cultures were dissociated using Accutase (Millipore) for 10 min and then isolated from differentiation cultures using magnetic activated cell sorting (Miltenyi Biotech) with an antibody against CD31 conjugated to magnetic microbeads. Isolated cells were then replated on collagen-coated plates (50 μg/mL BD for 1 h at 37°C) in endothelial cell growth media (Lonza).

iPS EC characterization

Using methods described elsewhere,[3] iPS ECs were seeded into a channel running through a three-dimensional (3D) collagen type I matrix. The endothelialized channel was subsequently exposed to a cocktail of proangiogenic factors in the form of a linear gradient.

Tissue harvesting, processing, and histology, and immunohistochemistry

Animals were sacrificed at various time points and tissue was harvested from the intraperitoneal space. Explants were fixed in 4% PFA for 48 h at 4°C, dehydrated in graded ethanol (50–100%), embedded in paraffin, and sectioned using a microtome (6 μm) for immunohistochemical staining. For gross visualization of tissue, sections were stained with hematoxylin

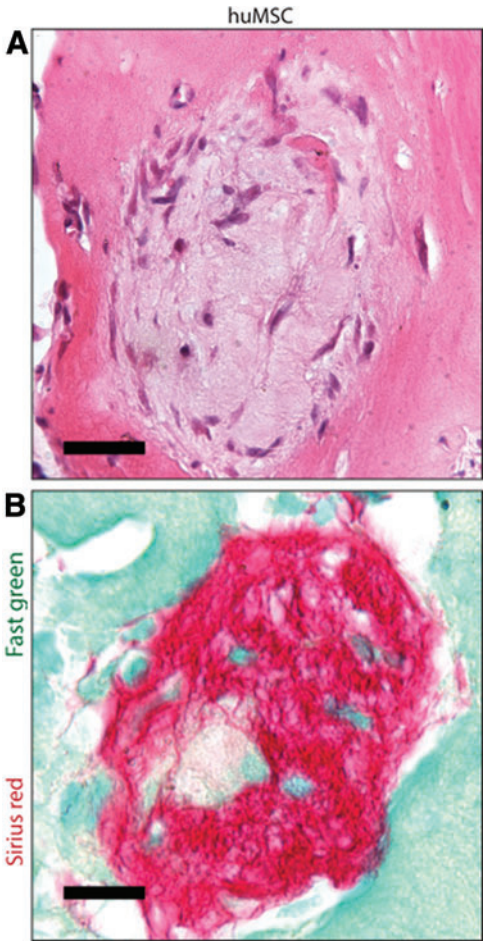

SUPPLEMENTARY FIG. S1. Human mesenchymal stem cell (MSC) cords. **(A)** Hematoxylin and eosin (H&E) staining of cords consisting of human MSCs resected after 7 days *in vivo* demonstrates the lack of red blood cells in cords lacking endothelial cells (scale bar, 50 μm). **(B)** Sirius red/fast-green staining of collagen within the cords after harvest (scale bar, 50 μm).

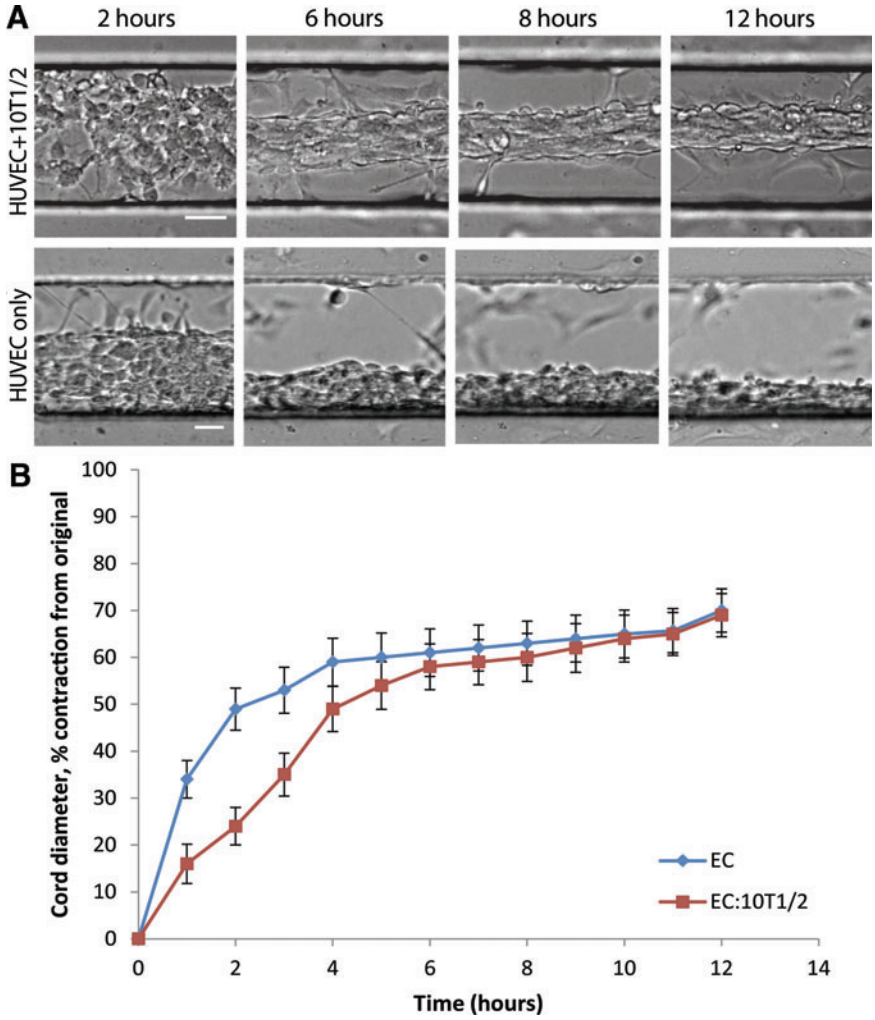

SUPPLEMENTARY FIG. S2. Coculture with 10T1/2s does not affect ultimate cord contraction *in vitro*. **(A)** Phase images of cord contraction of EC only and EC:10T1/2 (1:1) cords at 2, 6, 8, and 12 h of *in vitro* culture (scale bar, 50 μm). **(B)** Quantification of cord contraction at various time points. Error bars, SEM, $n = 5$.

and eosin (H&E). For identification of cords composed partially of collagen, sections were stained with Sirius red (collagen) and fast green (other tissue elements). For identification of vessels containing human endothelial cells, smooth muscle cells, and erythroid cells, sections were first blocked using the M.O.M. blocking reagent (Vector Labs) and normal goat serum and then immunostained using primary antibodies against human CD31 (1:20; Dako), Ter-119 (1:100; BD Biosciences), and smooth muscle alpha-actin (1:100; Abcam), respectively. A signal was visualized after incubation with secondary goat anti-IgG1-Alexa 555, goat anti-rat-Alexa 488, and donkey anti-rabbit-Alexa 647 antibodies (Jackson ImmunoResearch). For identification of primary hepatocytes adjacent to vessels containing red blood cells, sections were blocked using normal donkey serum, then incubated with primary antibodies against arginase-1 (ARG1, 1:400; Sigma-Aldrich) and Ter-119, and followed with species-appropriate secondary antibodies conjugated to Alexa 488 and 555. To visualize perfusion, a 200 μL solution of 100 μg/mL lectin from *Ulex europaeus* agglutinin (UEA-1) conjugated to TRITC (Vector labs) in PBS was injected intravenously through the tail vein. Animals were sacrificed and tissue was harvested from the graft site and processed for cryosectioning immediately after injection. Images were obtained using a Leica TCS SP5 Multiphoton and Spectral Confocal System with Hamamatsu 9624 Detector.

References

1. Si-Tayeb, K., Noto, F.K., Nagaoka. M., Li, J., Battle, M.A., Duris, C., North, P.E., Dalton, S., and Duncan, S.A. Highly efficient generation of human hepatocyte–like cells from induced pluripotent stem cells. Hepatology **51,** 297, 2010.
2. James, D., Nam, H.S., Seandel, M., Nolan, D., Janovitz, T., Tomishima, M., Studer, L., Lee, G., Lyden, D., Benezra, R., Zaninovic, N., Rosenwaks, Z., Rabbany, S.Y., and Rafii, S. Expansion and maintenance of human embryonic stem cell-derived endothelial cells by TGF [beta] inhibition is Id1 dependent. Nat Biotechnol **28,** 161, 2010.
3. Nguyen, D.H.T., Stapleton, S.C., Yang, M.T., Cha, S.S., Choi, C.K., Galie, P.A., and Chen, C.S. Biomimetic model to reconstitute angiogenic sprouting morphogenesis *in vitro*. Proc Natl Acad Sci U S A **110,** 6712, 2013.

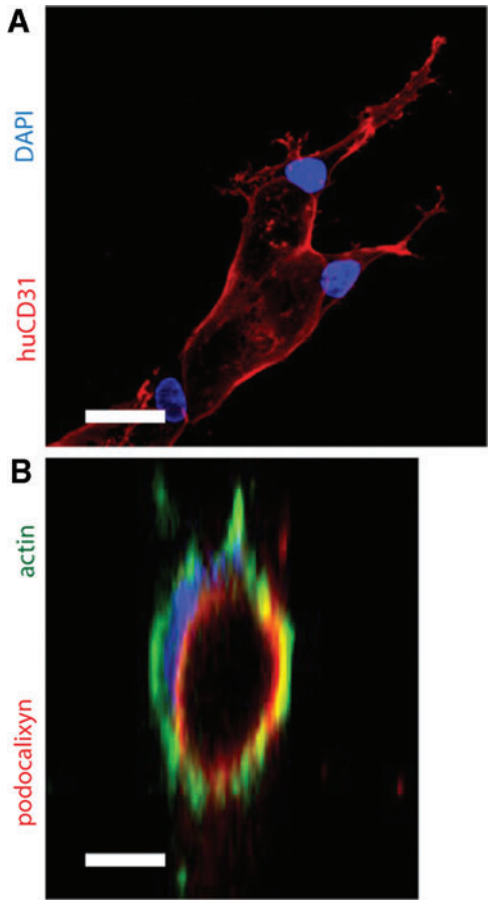

SUPPLEMENTARY FIG. S3. iPS ECs produce characteristic EC sprouts *in vitro*. **(A)** Representative confocal immunofluorescence image of a multicellular sprout stained for CD31 (*red*) and DAPI (*blue*) (scale bar, 25 μm). **(B)** Cross-section image of a sprout stained for podocalyxin (*red*), F-actin (*green*), and DAPI (*blue*) (scale bar, 15 μm).